SMOOTHING AND ADAPTIVE REDISTRIBUTION FOR GRIDS WITH IRREGULAR VALENCE AND HANGING NODES

Larisa Branets[1] Graham F. Carey[2]

CFDLab, ICES, The University of Texas at Austin, [1]*larisa@ices.utexas.edu*
[2]*carey@cfdlab.ae.utexas.edu*

ABSTRACT

We describe some extensions to the grid smoothing scheme described in [1, 2] that deal with the following issues: 1) the clustering effect of changing valence in an unstructured grid and, in particular, the choice of the shape and size control weighting both locally and globally; 2) an analysis of the angle bounds achievable through the new smoothing algorithm under shape control; 3) the extension of the approach to 3D with an application to a 3D grid generated by CUBIT; 4) the use of alternative metrics to provide clustering based on an approximate solution; 5) the treatment of constraints on boundaries and at hanging nodes introduced through adaptive refinement applied in conjunction with interior grid smoothing. The results of numerical studies are included to demonstrate the performance of the resulting schemes.

Keywords: mesh smoothing, adaptive redistribution, mesh quality metrics

1. INTRODUCTION

Grid generation and, in particular, the construction of "quality" grids is a major issue in both geometric modeling and engineering analysis. For realistic complex applications the analysis problem can usually be completed in less design time than the generation and improvement of a quality grid. In fact, it often takes an order of magnitude more time to construct a quality grid than to solve the analysis problem. Consequently, the problem of generating quality grids is becoming increasingly important.

Automatically generated grids frequently contain overlapping and distorted cells. A number of techniques have been directed towards smoothing the grid to correct these "abnormalities". Some of the earlier grid smoothing strategies are described in [3]-[9] and are based on both local relaxation of the grid and on global optimization strategies. Typically these earlier studies involve either geometric concepts associated with local cell quality such as the effect of obtuse angles or use variational ideas to optimize an associated functional. There have been several studies [10]-[12] that also focus on metrics to quantify cell quality and these have also been utilized in the grid improvement algorithms mentioned above.

The present approach is based on a global variational approach (optimization strategy) where the optimization functional utilizes local cell or patch properties associated with the map from an associated reference cell. Local contributions corresponding to both shape and size control determine grid quality via an associated weighted functional. In this work we investigate some of the properties of this weighted functional and explore extensions to treat certain complications.

An outline of the paper is as follows: In the first section we briefly review the local quality metric and variational problem. We then consider the effect of local changes in the valence (number of cells surrounding the grid vertex) and the use of variable weighting to avoid pathological behavior such as singular cluster-

ing due to local valence changes. Angle bounds of the shape control metric are developed and the extension of the scheme to 3D is described. Here we also consider the effect of distortion on the condition number for the subsequent analysis problem. In the closing sections we briefly describe the treatment of node constraints on the boundary and hanging node constraints in adaptive refinement as well as discuss one approach for adaptation with feedback from an analysis solution.

2. SMOOTHING TECHNIQUE

The variational smoothing algorithm we are developing was described in [1] and has its origins in several previous studies (see, for example, [3, 4, 6, 8, 13, 14]). As an introductory background, we first briefly outline the main idea of the approach below.

The method is based on a local cell distortion measure which is defined as a function of the Jacobian matrix S of a map between the reference and the physical cell. More specifically, it is a convex linear combination of measures of the element shape β and size distortion μ:

$$E_\theta(S) = (1-\theta)\beta(S) + \theta\mu(S), \quad 0 \le \theta < 1. \qquad (1)$$

E_θ takes values from the interval $[1, \infty]$. It achieves its minimum 1 on the reference element and becomes infinite on a degenerate element. The shape distortion part in n-dimensions is defined by

$$\beta(S) = \frac{\left(\frac{1}{n}\mathrm{tr}(S^T S)\right)^{n/2}}{\det S}. \qquad (2)$$

The size control part can be computed, using a target value v of the desired element area/volume defined *a priori*, and is

$$\mu(S) = \frac{1}{2}\left(\frac{\det S}{v} + \frac{v}{\det S}\right). \qquad (3)$$

The integral of (1) over the reference element $\hat{\Omega}_c$ is the element contribution

$$\mathcal{I}_c = \int_{\hat{\Omega}_c} E_\theta(S) d\vec{\xi} \qquad (4)$$

to the global distortion functional. The global variational grid smoothing functional is obtained by accumulating all N_c element contributions as:

$$\mathcal{I} = \sum_{c=1}^{N_c} \int_{\hat{\Omega}_c} E_\theta(S) d\vec{\xi} = \int_{\hat{\Omega}} E_\theta(S) d\vec{\xi}, \qquad (5)$$

where $\hat{\Omega}$ is a reference domain (union of all reference cells).

The functional (5) is minimized subject to related boundary (or other) constraints. The discretized form of the minimization problem (5) is: find the solution to

$$\mathbf{R} = \arg\min_{\mathbf{R}} \mathcal{I}_h, \quad \mathcal{I}_h = \sum_{c=1}^{N_c} \sum_{q(c)=1}^{N_q} \sigma_{q(c)} E_\theta(S|_{q(c)}), \quad (6)$$

where contributions to the functional from each cell c are approximated using a numerical integration rule with quadrature points $\{q(c)\}$, and quadrature weights $\sigma_{q(c)}$; $\mathbf{R}$ is the vector of "free" coordinates of vertices in the mesh.

3. VALENCE TREATMENT

Most, if not all, current smoothing algorithms produce significant local dilation effects at vertices where valence differs from the mean [1, 15]. The local valence of a vertex is defined here as a number of elements or cells that meet at that vertex. Since all unstructured grids have varying interior valence, we examine this case in detail.

Results from numerical tests in our previous works [1, 2] demonstrate that significant dilation may occur in such grids when smoothing with θ near zero; that is, with the accent on the shape control metric (similar results are seen for Laplacian-type smoothers). Increasing the size control θ alleviates this problem. It was also noticed that minimization of a global functional with more weight on shape control did not improve the minimal values of the quality metric and the Jacobian determinant compared to the initial state (although the global functional value was decreasing). That is, the value of such a functional depended more on the global mesh structure than on any individual cell contribution, as one might expect. On the other hand, when the weight was shifted towards the size control metric, all local quality metric values improved during smoothing. Thus, adding weight to the dilation metric makes our smoothing procedure less sensitive to the varying valence of the mesh. Nevertheless, we must always keep some nonzero weight on the shape control part of the metric in order to preserve the properties and validity of the smoothing algorithm. In the remainder of this section we will examine the effect of varying valence on both shape and size control parts of the functional.

3.1 Properties of the smoothing functional on meshes with changing valence.

We first examine the local behavior of the functional (6) on a patch of cells, then look at the global effect of smoothing on meshes with varying valence.

Patch of triangular elements Following [15], let us consider a patch of $val > 2$ equilateral triangular

elements shown in Figure 1 for the case $val = 6$.

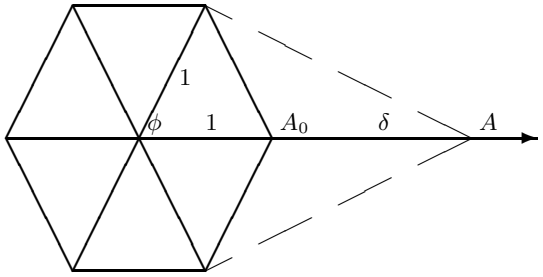

Figure 1: Patch of triangles.

For each element in the initial patch configuration we have

$$\phi = \frac{2\pi}{val}, \quad \beta_0 = \frac{2-\cos\phi}{\sqrt{3}\sin\phi}, \quad \mu_0 = \frac{v\sqrt{3}}{4\sin\phi} + \frac{\sin\phi}{v\sqrt{3}}.$$

Now we move one vertex A_0 a distance δ to a position A. The functional for the new patch depends upon δ

$$\mathcal{I}_h(\delta) = (val-2)E_\theta(0) + 2E_\theta(\delta).$$

Its derivative w.r.t. δ is equal to

$$\mathcal{I}'_h(\delta) = \frac{1}{\sqrt{3}\sin\phi}\left(2(1-\theta) + \frac{2\theta\sin^2\phi}{v} + \frac{4(\theta-1)-3\theta v}{2(1+\delta)^2}\right).$$

The minimum of this functional is achieved when $\mathcal{I}'_h(\delta) = 0$, that is when

$$\delta = \sqrt{\frac{1-(1-3v/4)\theta}{1-\theta+\theta/v\sin^2\phi}} - 1.$$

If $\theta = 0$ (only shape control is imposed), the minimum is at $\delta = 0$, independent of valence val. If $\theta = 1$ (only size control), the minimum is at $\delta = \sqrt{3}v/(2\sin\frac{2\pi}{val}) - 1$ and controlled by the value of desired element area v.

Patch of quadrilaterals The setting is similar to the previous case (see Figure 2)

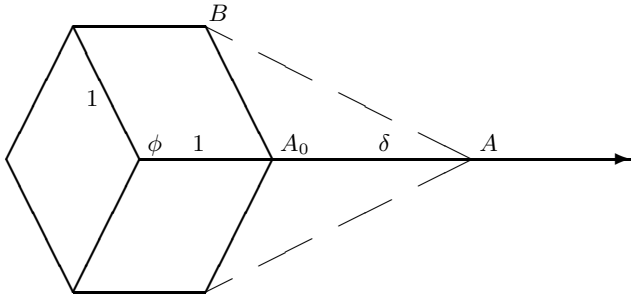

Figure 2: Patch of quadrilaterals.

and the functional becomes

$$\mathcal{I}(\delta) = (val-2)E_\theta(0) + \theta/2\left(\frac{v}{(1+\delta)\sin\phi} + \frac{(1+\delta)\sin\phi}{v}\right) +$$

$$+(1-\theta)/2\left(\frac{2+2(1+\delta)^2+\delta^2-2\delta\cos\phi}{2(1+\delta)\sin\phi} + \frac{\delta^2-2\delta\cos\phi}{2\sin\phi}\right),$$

with derivative

$$\mathcal{I}'_h(\delta) = \frac{1-\theta}{2\sin\phi}\left(3/2+\delta-\cos\phi-\frac{3/2+\cos\phi}{(1+\delta)^2}\right) +$$

$$+\frac{\theta}{2\sin\phi}\left(\frac{\sin^2\phi}{v} - \frac{v}{(1+\delta)^2}\right).$$

The contours $\mathcal{I}'_h(\delta) = 0$ as functions of valence val are shown in Figure 3 for different values of θ.

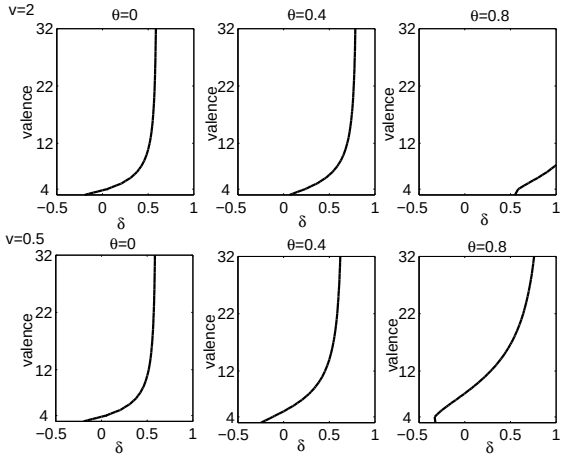

Figure 3: Optimal position δ as a function of valence and θ. On top: $v = 2$, on bottom: $v = 0.5$.

From Figure 3 we can conclude that smoothing of the quadrilateral grid with only shape control results in attraction of points to a node of valence smaller than regular and repulsion of points from a node of valence larger than regular. The same behavior holds for any Laplace-type smoothing. Addition of size control to the functional introduces control over this attraction/repulsion force through the values of desired element area v and parameter θ. Figure 3 also demonstrates that, as expected, large values of target cell area v induce dilation, whereas small values of v promote attraction. The effect is more dramatic with the increase of θ (weight shifted towards the size control part of the functional).

Functional at a node Now, let us consider an interior node of a quadrilateral grid in a different setting, where all nodes on the patch boundary are fixed and only the interior node is allowed to move. Let

us denote by $l_1, \ldots, l_{val}$ the lengths of all edges connected to this node. Let the angles between these edges be numbered in a counterclockwise manner as $\alpha_1, \ldots, \alpha_{val}$ (see Figure 4). The angles satisfy an ob-

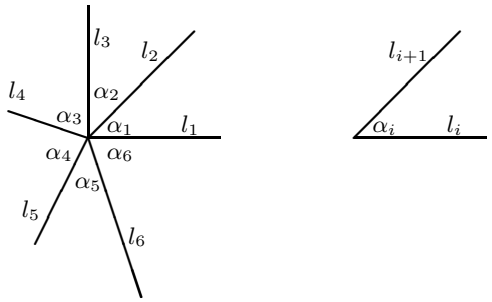

Figure 4: Interior node of valence $val = 6$.

vious restriction $\sum_{i=1}^{val} \alpha_i = 2\pi$. The functional value at the node is equal to

$$\mathcal{I}_h(\text{node}) = (1-\theta) \sum_{i=1}^{val} \frac{\frac{l_i}{l_{i+1}} + \frac{l_{i+1}}{l_i}}{2 \sin \alpha_i} +$$

$$\frac{\theta}{2} \sum_{i=1}^{val} \left(\frac{l_i l_{i+1} \sin \alpha_i}{v} + \frac{v}{l_i l_{i+1} \sin \alpha_i} \right)$$

and acheives its minimum value

$$\mathcal{I}_h(\text{node})_{\min} = (1-\theta) \frac{val}{\sin(\frac{2\pi}{val})} + \theta \; val$$

when $\alpha_1 = \ldots = \alpha_{val} = \frac{2\pi}{val}$ (due to symmetry) and $l_1 = \ldots = l_{val} = \sqrt{v / \sin(\frac{2\pi}{val})}$. Thus, such a symmetric configuration is preferable when it can be achieved under the given boundary and other constraints.

The position of any node influences the quality of the whole patch of cells surrounding the node. Suppose that in each cell of the patch the coordinates of three nodes (the interior node and two connected with it by edges) are determined by the conditions above. Let us consider the functional sensitivity to the position of the remaining vertices. It suffices to examine a typical cell. The level sets of the shape control metric β, as a function of coordinates of the fourth node (B in Figure 2) of a quadrilateral cell within the patch surrounding nodes with valence 3 and 5 are shown in Figure 5. In both cases the metric β has its minimum when the angle χ at the free vertex is equal to $\pi/2$. Thus, the edges forming this angle are forced to be 25% longer (than 1) in the case of the valence 3 patch and 17% shorter in the case of the valence 5 patch. Thus, the local dilation or contraction effect near points of irregular valence is caused by the tendency of a Laplace-type smoother to (1) preserve symmetry, (2) keep edge lengths nearly equal and (3) attain a maximum possible under these conditions amount of right angles in the mesh.

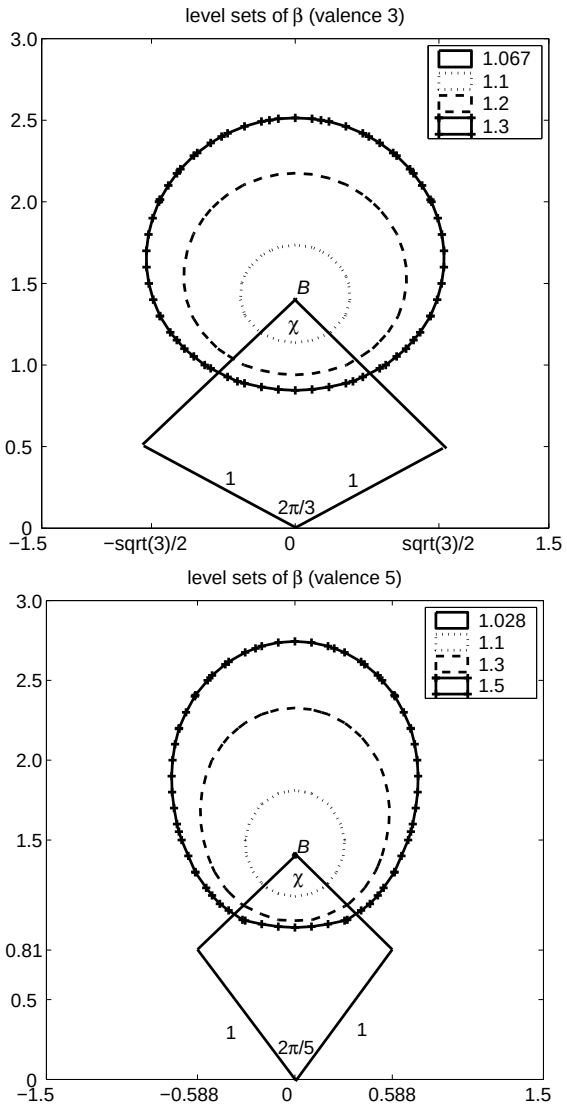

Figure 5: Level sets of β on a patch of valence 3 (top) and 5 (bottom).

If we now suppose that all other vertices in the grid have valence 4 and consider the layer of cells surrounding the irregular valence patch, similar reasoning implies that node clustering or unclustering near the point of irregular valence is due to the restriction on the sum of angles imposed by the global mesh connectivity. In order to demonstrate that in this case clustering is independent of the central (irregular valence) node contribution (even of the patch contribution), we performed smoothing of the test grid with deleted patches of cells surrounding valence 3 nodes. That is, we deleted the cells and considered different configurations of the resulting inner boundary. Smoothing is performed with value $\theta = 0.2$, and boundary nodes are allowed to "slide" tangentially along the outer boundary. The results for a coarse grid are shown in Figure 6. Similar behavior is displayed on finer grids.

In other situations, irregular valence nodes tend to induce mainly local dilation or contraction of the surrounding cells, as in the following example. In this case we consider a mesh of regular triangles and a uniform mesh of square cells in a big enough domain. That is, a domain big enough that boundaries do not affect the behavior of the smoother on the interior patches of interest. For the initial grid configuration we removed one node in the center for each of the two meshes and reconnected the remaining vertices (see Figure 7). Thus, we obtained several vertices of varying valence inside each mesh, with the majority of the vertices being of regular valence. The results of the smoothing for these meshes with different values of θ are shown in Figure 8, and in all these cases smoothing affects only the patches of cells surrounding the irregular valence vertices. That is, the effect of valence change attenuates significantly under this smoother and weighting.

This suggests that the effect of local valence irregularity can be addressed appropriately in this way. Hence, we anticipate the approach will improve element shape and not be impacted adversely by valence changes. This also suggests that local subgrid or patch optimization may be computationaly efficient. However, in general, the exterior mesh will vary globally unlike the uniform meshes of Figures 7 and 8.

3.2 Algorithm with varying θ.

One approach to deal with the valence problem is to introduce an alternative target shape for the cells located near the irregular valence nodes. The drawback of this approach is that we do not know which shape should be considered ideal for these cells (for example, what is the best configuration of the patch boundary in Figure 6?). A similar approach would be to enforce more size control near these irregular valence nodes and allow more shape control far from them. This can be achieved by varying parameter θ throughout the domain. Simply increasing or decreasing θ at a node with lower or higher valence is not enough. Our strategy is to identify the irregular valence nodes $v_i,\ i = 1, \ldots, I$, for each such node compute a radius of its "domain of influence" $r_{v_i} = \min_j\{\text{dist}(v_i, \partial\Omega), \frac{1}{2}\text{dist}(v_i, v_j)\}$, and define the piecewise-constant function θ on each cell by $\left\{\theta(c) = 1 - \frac{\text{dist}_{(v_i,c)}}{r_{v_i}},\ \text{if dist}(v_i, c) \le r_{v_i}\right\}$. The implementation of this approach resulted in the central grid shown in Figure 9. The grid obtained with varying θ does not show much clustering near valence 3 points, and it still has nearly square elements close to the boundary of the domain.

3.3 Bounds on angles

We conjecture that, in general, the maximum and minimum angles occur in the smoothed grid at the vertices with minimal (maximal) valence (excluding boundary influence). We do not have a proof of this yet, but we are able to obtain estimates on maximal and minimal angles in terms of distortion measure β for the case of triangular and tetrahedral grids, as described below. (Size distortion measure μ does not provide any control over the cells angles.)

For the triangular element with area A and edges $l_1 \le l_2 \le l_3$, the shape distortion measure is reduced to [1]

$$\beta = \frac{l_1^2 + l_2^2 + l_3^2}{4\sqrt{3}A}. \tag{7}$$

Let us denote the smallest angle by α_1, then we can rewrite the distortion measure as

$$\beta = \frac{l_2^2 + l_3^2 - l_2 l_3 \cos\alpha_1}{2\sqrt{3}A}.$$

For the sine of the smallest angle we, thus, have

$$\sin\alpha_1 = \frac{2A}{l_2 l_3} = \frac{l_2^2 + l_3^2 - l_2 l_3 \cos\alpha_1}{\sqrt{3}\beta l_2 l_3} \ge$$

$$\ge \frac{2 - \cos\alpha_1}{\sqrt{3}\beta}. \tag{8}$$

From the last inequality and using the fact that $\alpha_1 \le \pi/3$ it is easy to obtain the following estimate

$$\alpha_1 \ge \arcsin\left(\frac{2 - \sqrt{1 - \beta^{-2}}}{\sqrt{3}\beta + 1/(\sqrt{3}\beta)}\right). \tag{9}$$

For the largest angle α_3 in the triangle we can show (repeating (8)) the estimate

$$\sin\alpha_3 \ge \frac{2 - \cos\alpha_3}{\sqrt{3}\beta}.$$

If this angle is obtuse $\alpha_3 \ge \pi/2$ then

$$\sin(\pi - \alpha_3) \ge \frac{2 + \cos(\pi - \alpha_3)}{\sqrt{3}\beta}$$

and

$$\alpha_3 \leq \pi - \arcsin\left(\frac{2+\sqrt{1-\beta^{-2}}}{\sqrt{3}\beta + 1/(\sqrt{3}\beta)}\right). \qquad (10)$$

For the tetrahedron with volume V, solid angles $\gamma_1, \ldots, \gamma_4$, and edges $l_1, \ldots, l_6$ the shape distortion measure is [1]

$$\beta = \frac{(\sum_{i=1}^{6} l_i^2)^{3/2}}{72\sqrt{3}V}. \qquad (11)$$

Using the estimates from [16], for the minimal solid angle γ_1 we get

$$1/(16\beta) \leq \sin(\gamma_1/2) \leq \sqrt[4]{8}/\sqrt{\beta}.$$

Thus,

$$\gamma_1 \leq 2\arcsin\left(\frac{1}{16\beta}\right). \qquad (12)$$

From [16] we also know that

$$\gamma_1 \leq \gamma_2 \leq \gamma_3 \leq \gamma_4 \Rightarrow$$

$$\sin(\gamma_1/2) \leq \sin(\gamma_2/2) \leq \sin(\gamma_3/2) \leq \sin(\gamma_4/2).$$

The tetrahedron is poorly shaped if γ_4 is close to 2π, i.e. when $2\pi - \gamma_4$ is small. However, since

$$\sin\left(\frac{2\pi-\gamma_4}{2}\right) \geq \sin(\gamma_1/2),$$

consequently

$$\gamma_4 \leq 2\pi - 2\arcsin\left(\frac{1}{16\beta}\right), \qquad (13)$$

which shows how the largest value of distortion measure for the grid can be used to estimate the bounds on the smallest and largest angles.

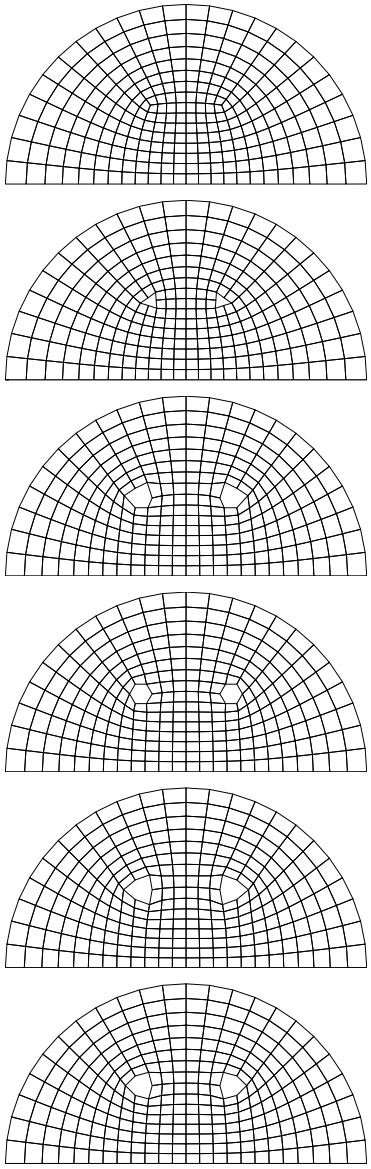

Figure 6: From top to bottom: whole smoothed grid, smoothed grid with free nodes on the boundaries of deleted patches, smoothed grid with patch boundaries fixed from initial grid, smoothed grids with vertex angle χ equal to 120, 80 and 90 degrees.

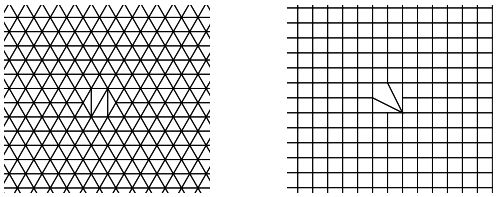

Figure 7: Zoom on the initial regular grids with one node removed.

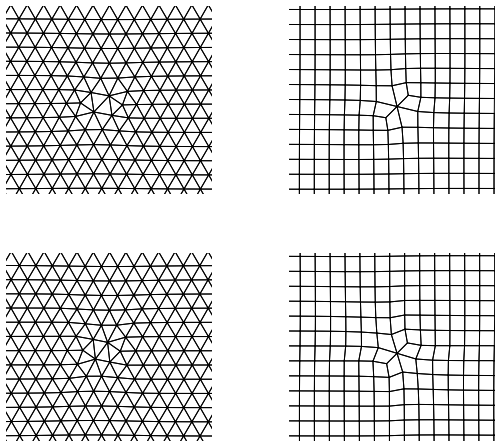

Figure 8: Zoom on the smoothed grids: on top $\theta = 0.2$, on bottom $\theta = 0.8$.

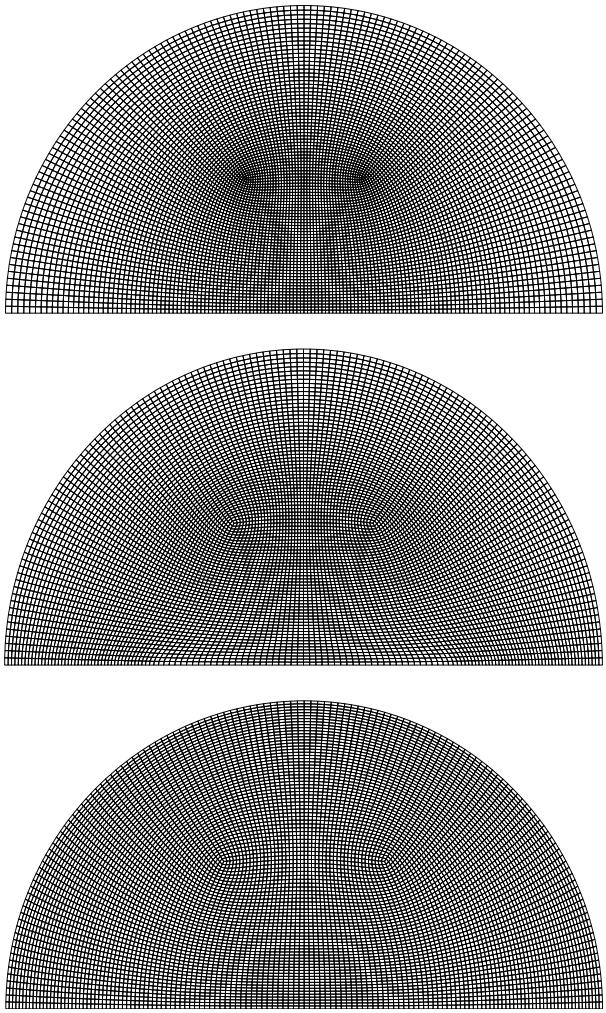

Figure 9: From top to bottom: grid smoothed with $\theta = 0.2$, varying θ, and $\theta = 0.8$.

4. 3D EXAMPLE

Now let us consider a 3D example of a grid with varying valence (Figure 10) that is comprised of hexahedra and genereted by CUBIT [17]. Obviously, all the difficulties discussed above for the 2D case are present here as well. The problem domain is composed of three tube segments that intersect as shown in Figure 10 and the main area of interest is the interior grid near the intersection. An expanded view of the 2D midplane slice near this area is shown on the right of the lower figure.

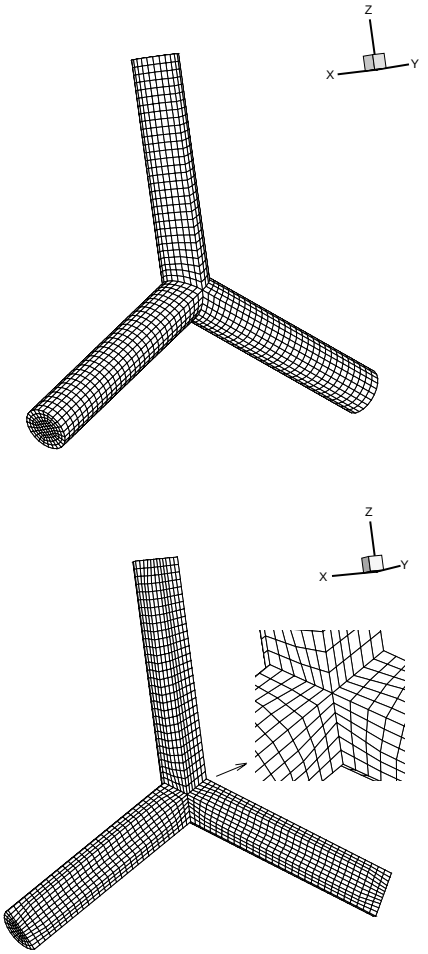

Figure 10: Initial 3D grid.

For this initial grid, the worst values of the Jacobian determinant and distortion measure are

$$\min\left(\det S\right)|_{q(c)} = 0.377v, \quad v = 1.1710^{-3},$$

$$\text{distortion } \max E_{0.8} = 1.63, \ \max E_{0.2} = 2.26,$$

$$\text{and } \beta_{0,\max} = 2.50, \quad \mu_{0,\max} = 1.51.$$

Since we want to have a practical understanding of the effect of mesh improvement on solvability after smoothing, we also compute the condition numbers for a representative mass matrix M and stiffness matrix K for the Laplace problem on the initial mesh. Dirichlet boundary conditions apply and both mass and stiffness matrices are symmetric positive definite. The associated condition numbers of the initial grid are

$$\kappa(M) = 35.51, \quad \kappa(K) = 44.31.$$

The interior grid on the section after smoothing with $\theta = 0.8$ (size control) is shown in Figure 11. The worst values of the Jacobian determinant and distortion measure are improved to

$$\min\left(\det S\right)|_{q(c)} = 0.48v, \ \max E_{0.8} = 1.39,$$

$$\beta_{\max} = 2.32, \quad \mu_{\max} = 1.27.$$

The condition numbers for mass and stiffness matrices

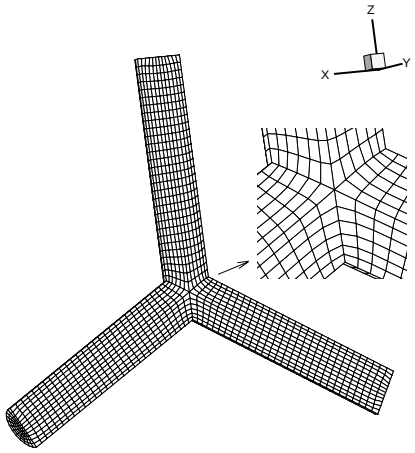

Figure 11: Grid slice after smoothing with $\theta = 0.8$.

become

$$\kappa_{0.8}(M) = 34.76 = 97\%\kappa(M),$$

$$\kappa_{0.8}(K) = 36.37 = 82\%\kappa(K).$$

The planar grid section after smoothing with $\theta = 0.2$ (shape control), is shown in Figure 12. The values now are

$$\min\left(\det S\right)|_{q(c)} = 0.377v, \ \max E_{0.2} = 2.20,$$

$$\beta_{\max} = 2.43, \quad \mu_{\max} = 1.52.$$

Condition numbers for mass and stiffness matrices become

$$\kappa_{0.2}(M) = 55.50 = 156\%\kappa(M),$$

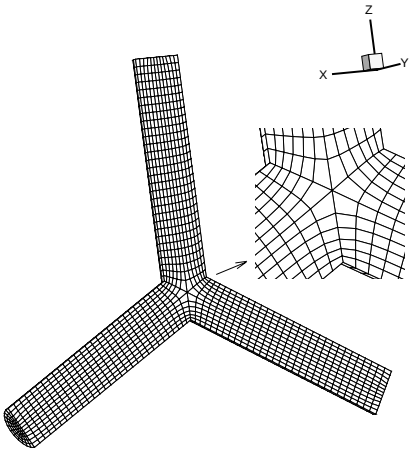

Figure 12: Grid slice after smoothing with $\theta = 0.2$.

$$\kappa_{0.2}(K) = 59.63 = 135\%\kappa(K).$$

The results follow the trend discussed in the beginning of Section 3 above; that is, smoothing with shape control does not improve the individual worst values of quality metric that occur near the irregular valence points. However, size control helps to improve all the values of quality. The conditioning of mass and stiffness matrices follows the behavior of the extremal values of quality and Jacobian determinant.

This observation leads us to develop the following theoretical estimates, concerning the relation between the maximum value of mesh quality E_θ and the conditioning of mass and stiffness matrices for that mesh. First recall that the mass matrix elements are computed as follows:

$$M_{i,j} = \sum_{c=1}^{N_c} \int_{\Omega_c} \varphi_i \varphi_j d\mathbf{x} = \sum_{c=1}^{N_c} \int_{\hat{\Omega}_c} \varphi_i \varphi_j \det S \, d\vec{\xi} = \tag{14}$$

$$= \sum_{c=1}^{N_c} \sum_{q(c)=1}^{N_q} \varphi_i(q)\, \varphi_j(q) \det S|_{q(c)} \sigma_{q(c)} =$$

$$= \left(\sum_{c=1}^{N_c} \sum_{q(c)=1}^{N_q} a_{q(c)} \det S|_{q(c)} \right) M^{ideal}_{i,j},$$

where M^{ideal} is a mass matrix computed on a reference mesh, φ_i, $i = 1, \ldots, N$ are the FE basis functions, and the constant coefficients $a_{q(c)} \geq 0$ satisfy $\sum_{c=1}^{N_c} \sum_{q(c)=1}^{N_q} a_{q(c)} = 1$. Thus, the i^{th} eigenvalue of the mass matrix satisfies

$$\max(\det S) \geq \frac{\lambda_i(M)}{\lambda_i(M^{ideal})} \geq \min(\det S), \tag{15}$$

and the condition number is bounded above as

$$\kappa(M) \leq \frac{\max(\det S)}{\min(\det S)} \kappa(M^{ideal}). \tag{16}$$

Similarly, the stiffness matrix elements can be written as:

$$K_{i,j} = \sum_{c=1}^{N_c} \int_{\Omega_c} (\nabla \varphi_i)^T \nabla \varphi_j d\mathbf{x} =$$

$$= \sum_{c=1}^{N_c} \int_{\hat{\Omega}_c} (\nabla_\xi \varphi_i)^T S^{-1} S^{-T} \nabla_\xi \varphi_j \det S \, d\vec{\xi}$$

and we have the bounds

$$\max\left(\frac{\det S}{\gamma^2 v^{2/n}}\right) \geq \frac{\lambda_i(K)}{\lambda_i(K^{ideal})} \geq \min\left(\frac{\det S}{\Gamma^2 v^{2/n}}\right), \tag{17}$$

where $K^{ideal}_{i,j}$ is a stiffness matrix computed on a reference mesh and by γ, Γ we denote the smallest and largest dimensionless singular values of the Jacobian matrix:

$$\gamma^2 v^{2/n} I \leq S^T S \leq \Gamma^2 v^{2/n} I. \tag{18}$$

Thus, the estimate for the condition number of the stiffness matrix is

$$\kappa(K) \leq \frac{\max\left(\frac{\det S}{\gamma^2}\right)}{\min\left(\frac{\det S}{\Gamma^2}\right)} \kappa(K^{ideal}). \tag{19}$$

From the definitions of μ in (3) and E_θ in (1) we get

$$\mu - \sqrt{\mu^2 - 1} \leq \det S / v \leq \mu + \sqrt{\mu^2 - 1},$$

$$\beta \leq \frac{E_\theta - \theta}{1 - \theta}, \quad \mu \leq \frac{E_\theta - 1 + \theta}{\theta}.$$

Also, from the definition of β in (2), it follows that

$$\left(\frac{1}{n} \mathrm{tr}(S^T S)\right)^{n/2} = \beta \det S \leq$$

$$\leq \beta_{\max} v (\mu_{\max} + \sqrt{\mu^2_{\max} - 1}).$$

Consequently,

$$\Gamma^n \leq n^{n/2} \beta_{\max} (\mu_{\max} + \sqrt{\mu^2_{\max} - 1}).$$

Thus, we can express the estimates for condition numbers (16) and (19) in terms of maximum values of β and μ, or, equivalently, in terms of maximum value of the distortion metric E_θ alone.

For the above example we estimate the change in the condition number of the mass matrix as follows

$$\kappa_{0.8}(M)/\kappa(M) = 74\%, \quad \kappa_{0.2}(M)/\kappa(M) = 142\%,$$

and for the stiffness matrix the estimated values (assuming $\Gamma\gamma = O(1)$) are

$$\kappa_{0.8}(K)/\kappa(K) = 77\%, \ \kappa_{0.2}(K)/\kappa(K) = 173\%.$$

These theoretical predictions are in qualitative agreement with the computed values. From these estimates we can conclude that, for a highly distorted grid ($E_\theta >> 1$), the condition number of the stiffness matrix is proportional to $(\max E_\theta)^{4/n}$.

5. TREATMENT OF CONSTRAINTS

Constraints on the grid points at boundaries, interfaces, or at hanging nodes in adaptive mesh refinement can be treated by multiplier methods in the variational smoothing formulation. In the following section, we briefly describe a Lagrange multiplier approach which is suggested for use in the cases mentioned above as a postprocessing step. That is, this step is to be applied after smoothing the grid (in n-dimensions) with hanging nodes as interior unconstrained nodes and boundary nodes as fixed. Let us define the Lagrangian for constraints $g_i(\mathbf{R}) = 0$ as

$$\mathcal{L}_h = \mathcal{I}_h + \sum_{i=1}^{NC} \lambda_i g_i(\mathbf{R}) = \mathcal{I}_h + \mathbf{\Lambda} G, \qquad (20)$$

where the number of constraints NC is equal to n times the number of hanging nodes plus the number of the "moving" boundary nodes. Here $\mathbf{\Lambda} = \{\lambda_i, i = 1, \ldots, NC\}$ are the discrete Lagrange multipliers. The minimization of the Lagrangian proceeds by a damped Newton method:

First specify the initial iterate $\begin{pmatrix} \mathbf{R} \\ \mathbf{\Lambda} \end{pmatrix} = \begin{pmatrix} \mathbf{R}^0 \\ \mathbf{0} \end{pmatrix}$

for $k = 0, 1, 2, \ldots$

Find minimization direction $\mathbf{P}^k$ from

$$\begin{pmatrix} \mathcal{H} & \mathcal{B} \\ \mathcal{B}^T & 0 \end{pmatrix} \begin{pmatrix} \mathbf{P}_R^k \\ \mathbf{P}_\Lambda^k \end{pmatrix} = \begin{pmatrix} -\nabla \mathcal{I}_h - \mathcal{B}\Lambda^k \\ -G \end{pmatrix},$$

where $\mathcal{B}(i,j) = \dfrac{\partial g_j}{\partial R_i}$; $\mathcal{H}(i,j) = \dfrac{\partial^2 \mathcal{L}_h}{\partial R_i \partial R_j}$;

Solve approximately

$$\tau_k = \arg\min_\tau \mathcal{L}_h \left(\begin{pmatrix} \mathbf{R}^k \\ \Lambda^k \end{pmatrix} + \tau \mathbf{P}^k \right);$$

$\mathbf{R}^{k+1} = \mathbf{R}^k + \tau_k \mathbf{P}_R^k$;

if $|\min_{q(c)} E_\theta^{-1}(\mathbf{R}^{k+1}) - \min_{q(c)} E_\theta^{-1}(\mathbf{R}^k)| < \epsilon$, stop.

The minimization direction can be computed using only the diagonal part of the Hessian $\mathcal{H}$ from the system

$$\begin{aligned} \mathcal{B}^T \mathcal{H}^{-1} \mathcal{B} \mathbf{P}_\Lambda &= -\mathcal{B}^T \mathcal{H}^{-1} \nabla \mathcal{I}_h - G; \\ \mathcal{H} \mathbf{P}_R &= -\nabla \mathcal{I}_h - \mathcal{B} \mathbf{P}_\Lambda. \end{aligned} \qquad (21)$$

For the 2D case, the $n = 2$ constraints $g_k = 0$ for a hanging node j with adjacent edge nodes p_1 and p_2 defining the constraint for j are given by

$$g_k = x_k(j) - \frac{x_k(p_1) + x_k(p_2)}{2}, \quad k = 1, 2.$$

For a "moving" boundary node j we first determine whether this node j and its neighbour boundary nodes $b_1, \ldots, b_{nb}$ lie on the same plane (line in 2D). In this case, the constraint forbids node movement in the normal direction $\mathbf{n}$

$$g_i = \sum_{k=1}^{n} (x_k^{new}(j) - x_k(j)) n_k.$$

For example, in 2D

$$n_1 = \frac{1}{x_1(b_1) - x_1(b_2)}, \quad n_2 = \frac{-1}{x_2(b_1) - x_2(b_2)}.$$

In the case of a nonzero curvature boundary, the node is allowed to move along the sphere (circle), going through node j and its boundary neighbours.

$$g_i = \sum_{k=1}^{nb} (x_k^{new}(j) - x_k(center))^2 - r^2.$$

Computation of this quadratic approximation to a surface requires a minimal number of nodes, although other forms (than the sphere/circle) might be preferable.

6. ADAPTIVITY AND MAPPING CONTROL

The shape control part of the functional (6) achieves its global minimum when the shape of each cell in the mesh is closest (under the given mesh connectivity and boundary constraints) to the shape of the reference cell. This is a necessary property for a smoothing algorithm, based on a "geometric" approach to element quality. On the other hand, one may define desired shape and size of the elements from the point of view of improving the accuracy of interpolation of a function or of approximating a solution to a FE problem. Such an approach is called adaptive redistribution, and in our case it can be achieved by describing the target shape and size of the cells in terms of an adaptive function.

6.1 Introduction of adaptivity into the smoothing formulation

One approach for adaptive mesh redistribution is to adaptively control the areas of the elements by introducing a weight function into the size control part of the quality metric. Examples of such techniques can be found in [4, 18, 19, 11, 9]. The use of several metric coefficients (instead of the single weight) improves the technique, since it allows for directional adaptation. The metric coefficient matrix $\mathcal{G}$ can be determined from the relation between the physical domain and an adaptive vector-function [20, 21, 8].

The previous variational problem, generalized for adaptation, is formulated as follows: minimize

$$\mathcal{I} = \int_{\hat{\Omega}} E_\theta(S\mathcal{G}^{1/2}) d\vec{\xi}. \qquad (22)$$

This problem is equivalent to the construction of a good quality mesh on the surface of values of an adaptive function and the result is the projection of this mesh onto the computational domain Ω.

We perform several exploratory numerical tests with a piecewise constant definition of the adaptive metric (see, for example [18, 13])

$$\mathcal{G} = \sqrt{1 + |\nabla u|^2}\, I,$$

where u is the adaptive function, I is the unit matrix. The role of $\mathcal{G}$ is to weight the integrand where $|\nabla u|$ is large. The shape control part β of the distortion measure is independent of this type of metric, so adaptive redistribution is due only to area (volume) change. Thus, the technique is equivalent to those described in the beginning of the section, since only desired element volume $v = v_0/\sqrt{1 + |\nabla u|^2}$ is dependent upon the adaptive function. In the tests, the initial grid is a uniform 3D hexahedral mesh inside the unit cube. Figure 13 shows horizontal layers of cells extracted from the middle section of the domain of redistributed grids.

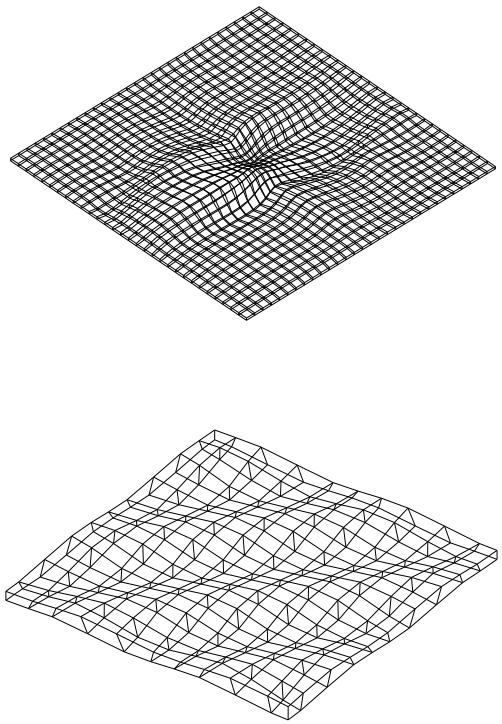

Figure 13: On top: adaptation to $u = \exp\left(-\frac{|x-0.5|+|y-0.5|+|z-0.5|}{\epsilon}\right)$, on bottom: adaptation to $u = \sin(2\pi(x+y+z))$.

6.2 Combining adaptive refinement and redistribution

We can expect that combination of r- and h-adaptivity will yield reduction in the number of degrees of freedom in the optimal mesh compared to the results of pure adaptive refinement. This approach will require the use of all smoothing algorithm extensions described in this paper. As an illustrative example we include Figure 14 which demonstrates the result of smoothing a mesh with hanging nodes and "sliding" boundary nodes with an adaptive metric.

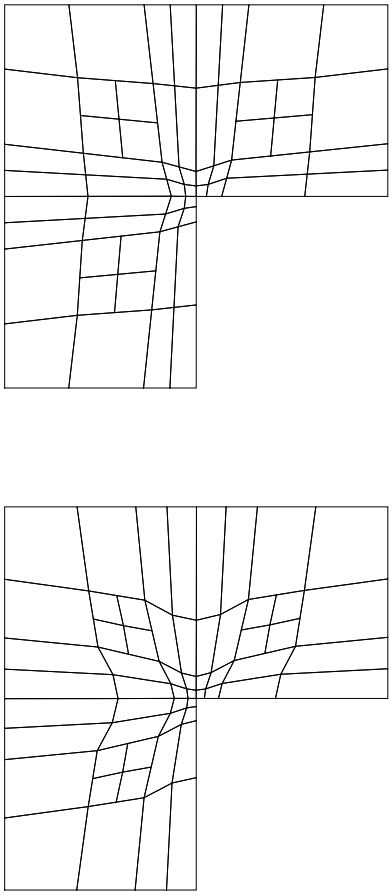

Figure 14: Adaptive smoothing step, on top: grid before smoothing, on bottom: smoothed grid.

7. CONCLUSIONS

In this study we have proposed and investigated several extensions to the grid smoothing strategy in [1, 2]. Specifically we investigate the effect of varying the weighting of shape and size control to address valence effects and demonstrate that the scheme can be adjusted to effectively treat the irregular valence issues

in both 2D and 3D grids. Theoretical bounds on the minimum and maximum angles for the triangular and tetrahedral grids and condition numbers estimates in terms of the distortion measure are obtained. The latter are shown to be consistent with results of a numerical test. In particular, this analysis implies that estimates improve when the described smoothing algorithm is applied. Finally, the idea of applying redistribution in conjunction with adaptive refinement has been implemented and some preliminary results are included for the L-shaped domain problem. In particular, we extend the metric to allow adaptive control based on the behavior of the solution to an associated approximation problem and we demonstrate the treatment of hanging nodes for problems where an adaptively refined grid is subsequently redistributed using this algorithm.

Acknowledgements: This study has been supported in part by LANL grant number 62485-001-03 and Sandia grant number 56522. We thank Bill Barth for contributing the initial CUBIT grid.

References

[1] Branets L., Carey G.F. "A Local Cell Quality Metric and Variational Grid Smoothing Algorithm." *Proceedings of the* 12^{th} *International Meshing Roundtable*, Sept. 2003

[2] Branets L., Carey G.F. "A Local Cell Quality Metric and Variational Grid Smoothing Algorithm." *Submitted to Engineering with Computers*

[3] Winslow A.M. "Numerical Solution of the Quasilinear Poisson Equation in a Nonuniform Triangle Mesh." *Journal of Computational Physics*, vol. 2, 149–172, 1967

[4] Brackbill J.U., Saltzman J.S. "Adaptive Zoning for Singular Problems in Two Dimensions." *Journal of Computational Physics*, vol. 46, 342–368, 1982

[5] Pardhanani A., Carey G.F. "Optimization of Computational Grids." *Numerical Methods for Partial Differential Equations*, vol. 4, 95–117, 1988

[6] Canann S.A., Stephenson M.B., Blacker T. "Optismoothing: An Optimization-driven Approach to Mesh Smoothing." *Finite Elements in analysis and Design*, vol. 13, 185–190, 1993

[7] Bank R.E., Xu J. "An algorithm for coarsening unstructured meshes." *Numerische Mathematik*, vol. 73, 1–36, 1996

[8] Charakhch'yan A.A., Ivanenko S.A. "A Variational Form of the Winslow Grid Generator." *Journal of Computational Physics*, vol. 136, 385–398, 1997

[9] Carey G.F. *Computational Grids: Generation, Adaptation and Solution Strategies.* Taylor and Francis, 1997

[10] Oddy A., Goldak J., McDill M., Bibby M. "A Distortion Metric for Isoparametric Finite Elements." *Trans. Can. Soc. Mech. Eng.*, vol. No. 38-CSME-32, Accession No. 2161, 1988

[11] Jacquotte O.P. "A Mechanical Model for a New Grid Generation Method in Computational Fluid Dynamics." *Computer Methods in Applied Mechanics and Engineering*, vol. 66, 323–338, 1987

[12] Knupp P. "Algebraic Mesh Quality Metrics." *SIAM Journal on Scientific Computing*, vol. 23, 193–218, 2001

[13] Garanzha V.A. "Barrier Variational Generation of Quasi-Isimetric Grids." *Computational Mathematics and Mathematical Physics*, vol. 40, 1617–1637, 2000

[14] Branets L.V., Garanzha V.A. "Global Condition Number of Trilinear Mapping. Application to 3D Grid Generation." *Proceedings of the minisymposium in the International conference "Optimization of finite-element approximations, splines and wavelets", June 25-29, St.-Petersburg, Russia*, 2001

[15] Brewer M. "Properties of the Element Condition Number Metric for Smoothing 2-D Meshes." *MS Thesis*, 2001

[16] Liu A., Joe B. "Relationship between Tetrahedron Shape Measures." *BIT*, vol. 34, 268–287, 1994

[17] Barth W. *Ph.D. Thesis, The University of Texas at Austin*, 2004

[18] Thompson J.F., Warsi Z.U.A., Mastin C.W. *Numerical grid generation.* North-Holland, New-York, 1985

[19] Anderson D.A. "Grid Cell Volume Control with an Adaptive Grid Generator." *Applied Mathematics and Computation*, vol. 35, 209–217, 1990

[20] Liseikin V.D. "On Construction of Uniform Grids on n-Dimensional Surfaces." *Computational Mathematics and Mathematical Physics*, vol. 31, 1670–1683, 1991

[21] Liseikin V.D. *Grid Generation Methods.* Springer-Verlag, Berlin, 1999